DOI: 10.61782/fa.2025.0945

FORUM ACUSTICUM
EURONOISE 2025

USING SPHERICAL ARRAY RECEIVERS TO EXTRACT SCATTERING COEFFICIENTS OF ROOM SURFACES

Xie, Dingding[1*] **Hornikx, Maarten**[1]

[1] Department of the Built Environment, Eindhoven University of Technology, P.O. Box 513 , Eindhoven , 5600 MB, the Netherlands

ABSTRACT

Scattering coefficients (SCs) are crucial for modeling room sound fields in rooms. Due to the lack of SCs on many practical surfaces and room objects, this study aims to derive a relation between surface SCs and the angular-dependent SCs obtained by a spherical receiver array in the room. The work is based on a computational approach. The sound field at a spherical receiver array is computed for a room with and without surface scattering at the room boundaries. A hybrid model of the Image Source Model and the Radiosity Model is used for this purpose. The sound field on the spherical receiver is then decomposed into plane waves, leading to ambisonic impulse responses (IRs). Then, the angular-dependent SCs are derived from these ambisonic IRs in both scenarios with a coherence method. Results show that angular-dependent SCs vary significantly depending on the apparent area of scattering surfaces as seen from the receiver, and a qualitative relationship between surface SCs and angular-dependent SCs is observed. This approach offers a promising framework for quantifying the scattering properties of room boundaries based on spherical array receivers.

Keywords: *scattering coefficient, image source model, radiosity model, directional property, coherence analysis.*

**Corresponding author*: *d.xie@tue.nl.*

1. INTRODUCTION

Scattering coefficients (SCs) are widely used in geometrical room acoustics modeling to quantify the ratio of incoherently reflected sound energy to total reflected energy on rough surfaces [1] [2]. In Ray Tracing (RT), SCs enable the modeling of surface scattering by either altering ray directions randomly or splitting rays upon interaction [3]. In hybrid models that combine the Image Source Model (ISM) with stochastic RT, SCs define the ratio between specular and diffuse reflection for each surface [4]. In hybrid ISM-radiosity models, SCs determine the energy deducted from the specular ISM component at each boundary element, redistributing it to nearby elements in the radiosity model for diffuse re-emission [5].

To determine SCs, both reverberation chamber and free-field methods can be used. A common approach involves mounting the test specimen on a turntable and measuring its surface under various orientations [1]. However, due to the challenge of measuring diverse surface types, SC databases remain limited. A simplified estimation method would be beneficial to approximate SC behavior across different surfaces, offering a practical alternative for SCs input room-acoustic simulations [6].

To develop a simplified SC estimation method, this research proposes measuring or simulating sound fields with spherical array receivers in reverberant environments under two conditions: with and without scattering surfaces installed. A coherence analysis of the sound fields in two scenarios is performed to extract angular-dependent SCs [7]. This study investigates the connection between **surface SCs** and **angular-dependent SCs**, demonstrating the potential for reverse-calculating surface SC from measured or simulated angular-dependent SCs in the future.

2. RESEARCH METHODS

Sound fields are simulated using geometrical acoustics models in a room with different boundary conditions: fully reflective (no scattering) and partially scattering. For both scenarios, the impulse responses (IRs) are sampled on a sphere and decomposed into plane waves [8], resulting in ambisonic IRs [9].

The ambisonic IRs are segmented into time intervals using a non-overlapping rectangular time window, yielding $p(N, t, \theta, \phi)$, where N is the time segment index and t is the time vector within the window. The window length corresponds to the travel time of one mean free path, calculated as [10]:

$$d = \frac{4V}{S}, \tag{1}$$

where V is the room volume and S is the total surface area. This approach ensures that each segment captures one mean free path order, represented by N.

The segmented ambisonic IRs for the rooms without and with scattering are denoted as $p_{wo}(N, t, \theta, \phi)$ and $p_w(N, t, \theta, \phi)$. Their corresponding frequency spectra are $P_{wo}(N, k, \theta, \phi)$ and $P_w(N, k, \theta, \phi)$. The coherence for each segment in a specific direction α [11],

$$\gamma_\alpha(N, k) = \frac{\left|\overline{P_{wo}(N, k, \theta, \phi) P_w^*(N, k, \theta, \phi)}\right|}{\left(\overline{|P_{wo}(N, k, \theta, \phi)|^2} \cdot \overline{|P_w(N, k, \theta, \phi)|^2}\right)^{0.5}}. \tag{2}$$

where * denotes the complex conjugate, and overline presents the average over all angles that have a cone angle with respect to α smaller than $pi/5$. By averaging over the wavenumber k, the coherence coefficient for each frequency band is obtained [7]:

$$\gamma_\alpha(N) = \overline{\gamma_\alpha(N, k)}. \tag{3}$$

The angular-dependent SC, s_α, quantifies the coherence loss of ambisonic IRs in the room with scattering relative to the room without scattering after one mean free path. The coherence coefficient can be related to the angular-dependent SC as [7] [12]:

$$\tilde{\gamma}_\alpha(N) = \sqrt{(1 - s_\alpha)^N}. \tag{4}$$

Finally, by fitting the simulated coherence coefficient $\gamma_\alpha(N)$ from Eq. (3) with the estimated $\tilde{\gamma}_\alpha(N)$ from Eq. (4), the s_α for each direction can be derived.

3. RESEARCH RESULTS

3.1 Room acoustics modeling

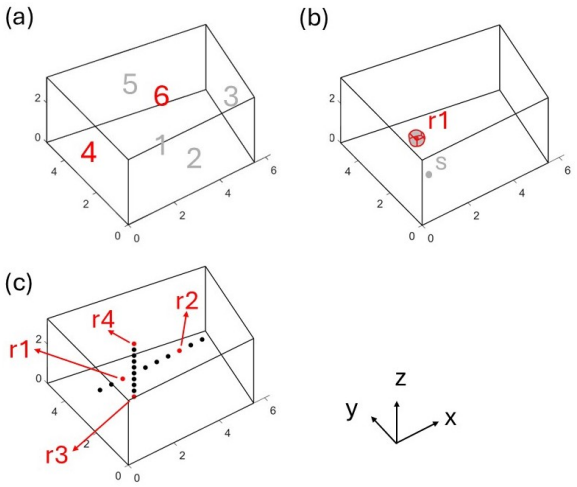

Figure 1. Room models (a) with wall indices marked, (b) with source and receiver position r1 illustrated, (c) with receiver arrays illustrated.

The room model depicted in Fig. 1 has a volume of 88.87 m^3 and a surface area of 123.17 m^2. The mean-free path length is 2.89 m. This model is simulated using the ISM under fully reflective conditions and the Combined Acoustical Radiosity–Image Source Method (CARISM [5]) for scenarios with partial scattering. The indices of each wall are shown in Fig. 1(a). All the walls have identical absorption coefficients of 0.2.

Table 1. Configurations of the source positions and receiver center positions.

Name	Code	Position (m)
source	s	[1.0,1.0,1.2]
receiver 1	r1	[1.5,2.5,1.5]
receiver 2	r2	[4.0,2.5,1.5]
receiver 3	r3	[2.0,2.5,0.3]
receiver 4	r4	[2.0,2.5,3.0]

An open spherical receiver array with a radius of 0.049 m, consisting of 20 receivers, is positioned at r1, as illustrated in Fig. 1(b), alongside a point source. In

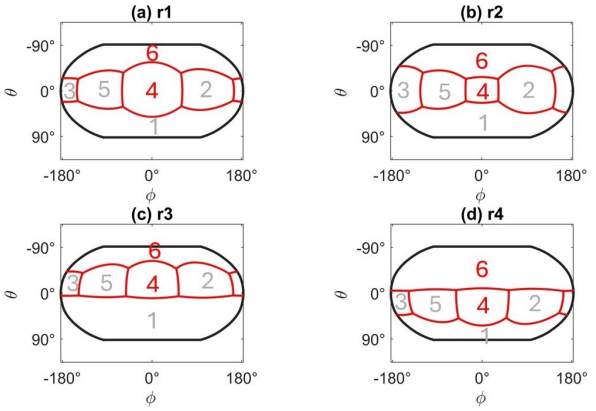

Figure 2. Wall edge projections on the receiver sphere with respect to (a) r1, (b) r2, (c) r3, and (d) r4.

Fig. 1(c), 10 receiver positions are selected along the x-axis and 10 along the z-axis. Four receiver positions, labeled r1 to r4, are highlighted in red and later used for demonstration purposes. The coordinates of the source and receiver center positions are provided in Tab. 1. From the perspective of these four receiver arrays, the projection of the wall edges onto each receiver sphere is shown in Fig. 2.

3.2 Coherence analysis

Taking r1 as an example, Fig. 3(a) illustrates the ambisonic IRs for the direction of the sound source across the 1000 Hz to 2500 Hz frequency range. Two scenarios are plotted: (i) all boundaries are fully reflective, and (ii) all boundaries have SCs of 0.3, i.e., $s_{w1:6} = 0.3$, where $w1:6$ represents walls 1 to 6. The signal is segmented using a sliding time window approach with no overlap, with each segment corresponding to a mean free-path order, as indicated by the vertical lines.

To compute coherence coefficients, the ambisonic IRs from directions adjacent to the source direction are utilized, following the method in the previous section. Fig. 3(b) presents the coherence coefficients, $\gamma_\alpha(N)$, for the source direction within this frequency band, up to the fifth order, shown as black dot-dash lines. The red curve in Fig. 3(b) represents the fitted coherence coefficients, $\tilde{\gamma}_\alpha(N)$, with a fitting parameter of $s_\alpha = 0.26$ for this direction. This process is repeated for different directions, yielding angular-dependent SCs across all directions.

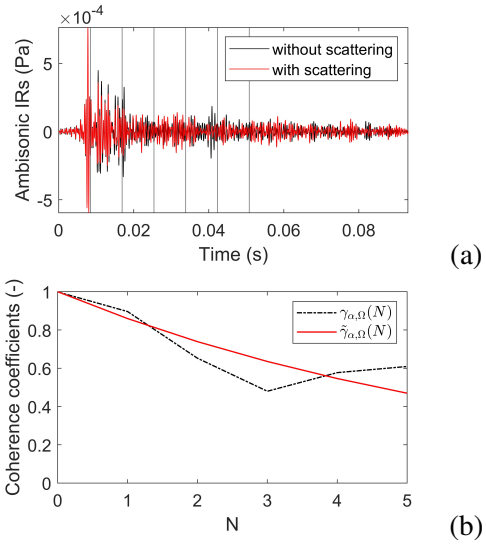

Figure 3. In the frequency band of 1000 Hz to 2500 Hz and in the direction of the source, (a) ambisonic IRs in the room with and without scattering, and (b) coherence coefficient curve $\gamma_\alpha(N)$ and its fitted curve $\tilde{\gamma}_\alpha(N)$.

3.3 Angular-dependent Scattering Coefficient

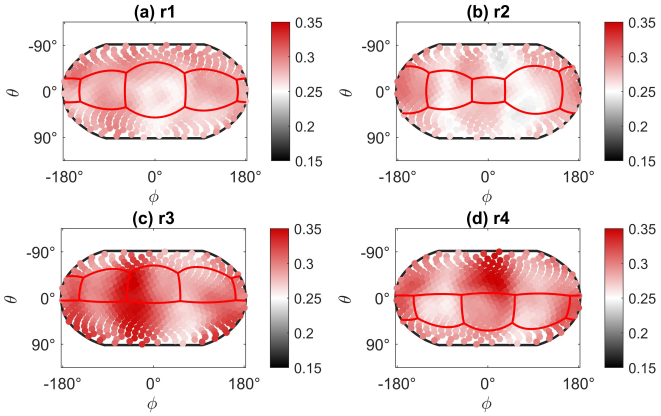

Figure 4. Angular-dependent SCs of room with $s_{w1:6} = 0.3$ at (a) r1, (b) r2, (c) r3, and (d) r4.

The obtained s_α values are plotted against angles to illustrate the degree of scattering in each direction from the receiver's perspective under three different boundary conditions, as detailed below. Additionally, the projections

of the wall edges onto each receiver sphere, as shown in Fig. 2, are included in these figures for clarity.

1. **Uniform Scattering**: All boundaries have a SC of 0.3 ($s_{w1:6} = 0.3$), as shown in Fig. 4.

2. **Localized Scattering on Wall 4**: Wall 4 has a SC of 0.9, while all other walls have a SC of 0 ($s_{w4} = 0.9$, $s_{w\neq w4} = 0$), as shown in Fig. 5.

3. **Localized Scattering on Wall 6**: Wall 6 has a SC of 0.9, while all other walls have a SC of 0 ($s_{w6} = 0.9$, $s_{w\neq w6} = 0$), as shown in Fig. 6.

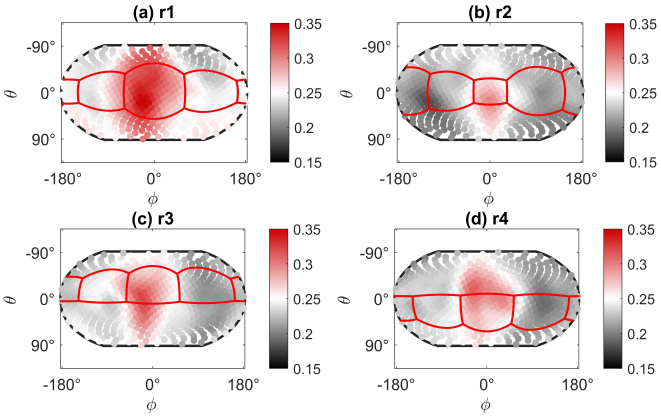

Figure 5. Angular-dependent SCs of room with $s_{w4} = 0.9$, $s_{w\neq w4} = 0$ at (a) r1, (b) r2, (c) r3, and (d) r4.

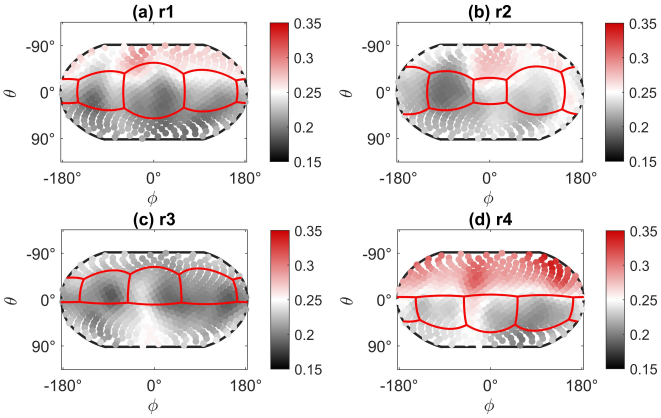

Figure 6. Angular-dependent SCs of room with $s_{w6} = 0.9$, $s_{w\neq w6} = 0$ at (a) r1, (b) r2, (c) r3, and (d) r4.

In Scenario 1, scattering is uniformly distributed across all boundaries, leading to relatively consistent angular-dependent SCs distributions, regardless of the receiver position, as shown in Fig. 4. The angular-dependent SCs remain close to 0.3 in most directions, aligning well with the surface SC. The angular-dependent SCs for r3 and r4 are slightly higher than those for r1 and r2.

However, when the scattering is unevenly distributed along the boundaries, the angular-dependent SCs extracted by the spherical array receivers behave differently from the surface SCs, as shown in Fig. 5 and Fig. 6. Receiver positions r1 and r2 are aligned horizontally, while r3 and r4 are aligned vertically.

In Scenario 2, only wall 4 has an SC of 0.9. As shown in Fig. 5, a higher degree of scattering is observed in the direction of wall 4, regardless of the receiver position. This is particularly evident from the perspective of r1, where wall 4 has the largest apparent area (projection area) compared to the other receiver positions, making the effect most pronounced. In contrast, at r2, which is farther from wall 4, wall 4 has the smallest apparent area, resulting in lower angular-dependent SCs in the direction of wall 4.

As for Scenario 3, only wall 6 (the ceiling) has a SC of 0.9. In Fig. 6(a) and (b), a higher degree of scattering is observed in the direction of the ceiling. In comparison to r1 and r2, r3 is positioned lower and farther from the ceiling, resulting in a scattering pattern with less distinct features. Meanwhile, r4 is closer to the ceiling, apparent area of the ceiling is larger, making the scattering from the ceiling more pronounced at this position, leading to a more noticeable scattering in the direction of the ceiling.

In the last two scenarios with uneven scattering distributions, we observe in directions where the surface SC is 0.9, angular-dependent SCs much lower than 0.9, and in directions where the surface SC is 0, angular-dependent SCs higher than 0. This is because angular-dependent SCs measure the scattering level in each direction as the overall effects of the room from the perspective of the receivers, rather than measuring a property of the surfaces. Therefore, it is not appropriate to directly map the angular-dependent SCs on the boundaries for use as surface SCs. To extract SCs of room surfaces using angular-dependent SCs, further quantitative connections between the two should be established in the future.

3.4 Angular-averaged Scattering Coefficient

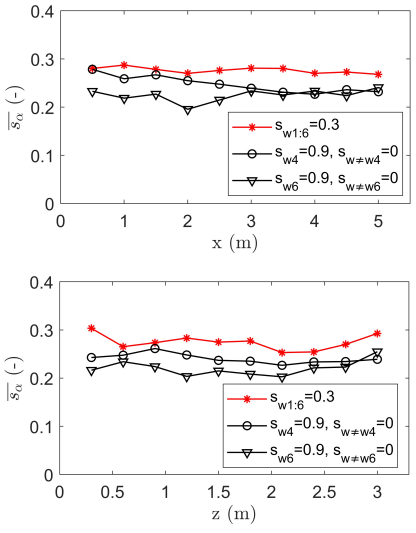

Figure 7. Angular-averaged SCs varying along (a) x-axis and (b) z-axis.

Two arrays, each composed of 10 spherical receivers, are shown in Fig. 1(c): one is aligned along the x-axis, spanning 0.5 m, and the other is aligned along the z-axis, spanning 0.3 m. The angular-dependent SCs are calculated for each position within the 1000 Hz to 2500 Hz frequency band and averaged over angles, resulting in the angular-averaged SCs $\overline{s_\alpha}$ at each receiver position. Fig. 7 shows how the angular-averaged SCs vary along the x-axis and z-axis. Overall, the angular-averaged SCs vary with receiver positions but are not highly sensitive to them [7].

With s_i and A_i representing the SC and surface area of the i_{th} surface, respectively, the room-averaged surface SC $\bar{s}$ is defined as [13]

$$\bar{s} = \frac{\sum s_i A_i}{\sum A_i}. \tag{5}$$

Under the boundary condition where a single SC of 0.3 is assigned to all boundaries, the angular-averaged SCs $\overline{s_\alpha}$ at these receiver positions are approximately equal to the room-averaged surface SC $\bar{s}$, demonstrating the effectiveness of the proposed method.

For the other two boundary conditions, although the scattering is highly unevenly distributed, the angular-averaged SCs remain relatively stable compared to the obvious variations in angular-dependent SCs. Particularly, in Fig. 7(a), when $s_{w4} = 0.9$, the $\overline{s_\alpha}$ is slightly higher when the receiver is closer to wall 4.

According to Eq. (5), the room-averaged surface SC $\bar{s}$ is 0.13 for Scenario 2 and 0.19 for Scenario 3. Notably, in Scenario 2, there is a relatively large discrepancy between room-averaged surface SC $\bar{s}$ and the angular-averaged SC $\overline{s_\alpha}$. The reasons for this difference require further investigation.

4. CONCLUSION

This study introduces a method for extracting angular-dependent SCs using spherical array receivers in reverberant environments. Utilizing a hybrid model combining the Image Source Model and the Radiosity Model, it finds the qualitative relationship between angular-dependent SCs from the receiver's perspective and the SCs of room surfaces. The results indicate that when scattering is uniformly distributed across all surfaces, angular-dependent SCs remain relatively consistent regardless of receiver position. In contrast, when scattering distributes unevenly on surfaces, angular-dependent SCs are higher in directions with greater surface scattering and are influenced by the apparent area of scattering surfaces visible to the receiver. However, angular-averaged SCs remain less sensitive to receiver location, regardless of whether the scattering is uniformly distributed.

Future work should further explore the quantitative relationship between surface SCs and angular-dependent SCs. Developing a method to reverse-calculate surface SCs from measured or simulated angular-dependent SCs will be beneficial for advancing a simplified SC estimation approach.

5. ACKNOWLEDGMENTS

We acknowledge Wouter Wittebol for his support with the Image Source Model and George Koutsouris for his support with the Radiosity Model.

6. REFERENCES

[1] M. Vorländer and E. Mommertz, "Definition and measurement of random-incidence scattering coefficients," *Applied Acoustics*, vol. 60 (2), 2000.

[2] T. Cox, B. Dalenback, P. D'Antonio, J. Embrechts, J. Jeon, E. Mommertz, and M. Vorländer, "A tutorial on scattering and diffusion coefficients for room

acoustic surfaces," *Acta acustica united with Acustica*, vol. 92 (1), 2006.

[3] L. Savioja and U. P. Svensson, "Overview of geometrical room acoustic modeling techniques," *J. Acoust. Soc. Am.*, vol. 138 (2), 2015.

[4] A. Wabnitz, N. Epain, C. Jin, and A. van Schaik, "Room acoustics simulation for multichannel microphone arrays," *Proceedings of the International Symposium on Room Acoustics*, 2010.

[5] G. I. Koutsouris, J. Brunskog, C.-H. Jeong, and F. Jacobsen, "Combination of acoustical radiosity and the image source method," *J. Acoust. Soc. Am.*, vol. 133 (6), 2013.

[6] M. Vorländer and S. Feistel, "Show your scattering coefficients," *183rd Meeting of the Acoustical Society of America*, 2022.

[7] D. Xie, W. Wittebol, Q. Li, and M. Hornikx, "A method for extracting an average scattering coefficient for room acoustic modeling," *Applied Acoustics*, vol. 233, p. 110604, 2025.

[8] B. Rafaely, *Fundamentals of spherical array processing*. Berlin Heidelberg: Springer, 2015.

[9] B. Alary, A. Politis, S. Schlecht, and V. Välimäki, "Directional feedback delay network," *J. Audio Eng. Soc.*, vol. 67 (10), pp. 752–762, 2019.

[10] H. Kuttruff, *Room Acoustics*. 6th ed., Boca Raton: CRC Press, 2017.

[11] F. Jacobsen and T. Roisin, "The coherence of reverberant sound fields," *J. Acoust. Soc. Am.*, vol. 108 (1), 2000.

[12] W. Wittebol, H. Wang, M. Hornikx, and P. Calamia, "A hybrid room acoustic modeling approach combining image source, acoustic diffusion equation, and time-domain discontinuous galerkin methods," *Applied Acoustics*, vol. 223, 2024.

[13] T. Hanyu, "A theoretical framework for quantitatively characterizing sound field diffusion based on scattering coefficient and absorption coefficient of walls," *J. Acoust. Soc. Am.*, vol. 128, 2010.